ChemSusChem

Research Article
doi.org/10.1002/cssc.202201847

Chemistry Europe
European Chemical Societies Publishing

www.chemsuschem.org

Methodological Studies of the Mechanism of Anion Insertion in Nanometer-Sized Carbon Micropores

Connor Welty,[a] Erin E. Taylor,[a] Sadie Posey,[a] Patric Vailati,[b, c] Kostiantyn V. Kravchyk,*[b, c] Maksym V. Kovalenko,[b, c] and Nicholas P. Stadie*[a]

Dual-ion hybrid capacitors (DIHCs) are a promising class of electrochemical energy storage devices intermediate between batteries and supercapacitors, exhibiting both high energy and power density, and generalizable across wide chemistries beyond lithium. In this study, a model carbon framework material with a periodic structure containing exclusively 1.2 nm width pores, zeolite-templated carbon (ZTC), was investigated as the positive electrode for the storage of a range of anions relevant to DIHC chemistries. Screening experiments were carried out across 21 electrolyte compositions within a common stable potential window of 3.0–4.0 V vs. Li/Li$^+$ to determine trends in capacity as a function of anion and solvent properties. To achieve fast rate capability, a binary solvent balancing a high dielectric constant with a low viscosity and small molecular size was used; optimized full-cells based on $LiPF_6$ in binary electrolyte exhibited 146 Wh kg^{-1} and >4000 W kg^{-1} energy and power densities, respectively.

Introduction

Dual-ion batteries (DIBs) are a class of electrochemical energy storage devices that are under serious consideration for the replacement of lithium-ion batteries (LIBs) in specific applications, especially for stationary storage.[1] Such cells comprise a negative and positive electrode, which undergo reversible insertion or intercalation of the cations and anions upon charging, respectively, which are initially present in the electrolyte. A possible benefit of DIBs over LIBs is their accommodation of diverse anions and cations beyond Li$^+$, where the latter is especially appealing for the future sustainability of battery production.[2] Graphite is commonly used as one or both electrodes in a DIB, where the latter case is often referred to as a dual-graphite battery. Anion intercalation in graphite (e.g., by PF_6^-), which typically occurs at high potentials relative to metal plating and stripping reactions, has been shown to be effective for achieving high cell voltage (and therefore high energy density).[3] In all cases, a DIB functions in distinct contrast to a standard LIB wherein Li$^+$ ions shuttle back and forth from one electrode to the other (and the anion plays a relatively minor role in overall charge/discharge cycling), referred to as a rocking-chair charge storage mechanism.[4] Dual-ion hybrid capacitors (DIHCs) consist of a carbonaceous material at one of the electrodes that undergoes capacitive charge storage at its surface instead of faradaic intercalation. Such hybrid capacitors typically exhibit high rate capability and charge/discharge reversibility.[5] Porous carbon is an attractive alternative to graphite as a positive electrode material owing to a similarly high working potential and the ability to accommodate large anions.[6]

In a typical DIB, the bare cation and anion are reversibly inserted/intercalated at the negative and positive electrode, respectively, undergoing desolvation at each electrode/electrolyte interface.[7–9] However, it is also possible that one or both relevant ions is co-inserted along with the solvent, sometimes leading to irreversible insertion of just the solvent (as in pillared graphite intercalation compounds).[7,10,11] An example of such behavior is the co-intercalation of PF_6^- along with propylene carbonate (PC), which has been found to occur at high voltages (5.2 V vs. Li/Li$^+$) to form the stage-I compound $C_{24}PF_6(PC)_4$.[12,13] It has subsequently been determined that PF_6^- can be co-intercalated into graphite in much higher ion/solvent ratios, up to 1:0.7±0.2 at the same plateau of 5.2 V using ethyl methyl carbonate (EMC) as the solvent.[13] At lower potentials, irreversible insertion of the solvent occurs during the first cycle co-insertion of PC and Li$^+$ into graphite at around 1.0 V vs. Li/Li$^+$, leading to the formation of a pillared graphite electrode as well as the exfoliation of the graphite, which changes the potential at which all subsequent insertion/deinsertion occurs.[12] Hence, the use of a three-dimensionally connected graphene-like

[a] C. Welty, E. E. Taylor, S. Posey, Prof. N. P. Stadie
Department of Chemistry & Biochemistry
Montana State University
PO Box 173400, Bozeman, MT 59717 (United States)
E-mail: nstadie@montana.edu
[b] P. Vailati, Dr. K. V. Kravchyk, Prof. M. V. Kovalenko
Laboratory for Thin Films and Photovoltaics
Empa-Swiss Federal Laboratories for Materials Science and Technology
Überlandstrasse 129, 8600, Dübendorf (Switzerland)
[c] P. Vailati, Dr. K. V. Kravchyk, Prof. M. V. Kovalenko
Laboratory of Inorganic Chemistry
ETH Zürich
Vladimir-Prelog-Weg 1, 8093, Zurich (Switzerland)
E-mail: kravchyk@inorg.chem.ethz.ch

Supporting information for this article is available on the WWW under https://doi.org/10.1002/cssc.202201847

This publication is part of a collection of invited contributions focusing on "Dual-Ion Batteries". Please visit chemsuschem.org/collections to view all contributions.

scaffold is an important candidate strategy toward preventing such issues.

Recently, numerous examples of DIHCs have been reported that explore combinations of metal plating/stripping reactions at the negative electrode with capacitive ion storage at high potentials at the positive electrode.[14] Several metals have been explored, including abundant, energy-dense elements such as sodium, magnesium, and aluminum.[15,16] The anions explored have varied across a wide range of weakly coordinating polyatomic species.[17] The solvent must be chosen to maximize the concentration of the salt since the energy density of a DIHC depends directly on the composition of the electrolyte.[18] Ionic liquids have also been explored, such as 1-butyl-1-methylpiperidinium bis(trifluoromethylsulfonyl)imide ($PP_{14}TFSI$) and *N*-butyl-*N*-methylpyrrolidinium bis(trifluoromethanesulfonyl)imide ($Pyr_{14}TFSI$).[6,19] In general, such cells can achieve appreciable energy densities and power densities concurrently, and efforts are underway to improve anion capacity and to increase and flatten the potential of anion adsorption on the positive side. However, each study is typically a one-off (or side-by-side comparison) of a single (or a few) thoroughly investigated electrode-electrolyte system(s).

Zeolite-templated carbon (ZTC) is a class of ordered microporous carbon materials of interest for capacitive charge storage applications owing to its high surface area and dense network of three-dimensionally connected, electrically conductive channels.[20] The pores are isotropically connected owing to the high symmetry of the zeolite template in which the framework is formed; the repeat distance between pores is 14 Å and the N_2 accessible pore width is around 12 Å, indicating that the molecular-sized channels are separated by atomistically thin carbon walls. Its three-dimensionally connected framework of graphene ribbon-like struts is locally disordered but exhibits long-range pore-to-pore ordering, uniquely enabling the construction of an accurate periodic model.[21] Upon systematic comparison of the numerous such models of ZTC to the experimental properties of the as-synthesized materials, it is possible to deduce that nearly around 80% of the volume of the bulk ZTC framework is accessible to small molecular adsorbates such as small molecular gases and ions.[22] This void volume is double that of highly porous zeolites ($\leq$40%) and equivalent to highly porous metal–organic frameworks (e.g., 82% for MOF-177); that is, no region of the material structure is off-limits to guests except its atomistically-thin graphene ribbon struts (see Figure 1a). Importantly, no part of the ZTC structure contains graphitic stacking and hence faradaic intercalation via staging is impermissible.

ZTCs have been investigated as the positive electrode material in several DIB/DIHC chemistries, including for chloroaluminate ($AlCl_4^-/Al_2Cl_7^-/Cl^-$) anion storage[23] and bis(fluorosulfonyl)imide (FSI^-) anion storage,[24] as well as for divalent magnesium (Mg^{2+}) cation storage in a type of Mg-ion hybrid capacitor (MHC).[25] The maximum reversible capacity observed (under varying conditions) in each cell type was 382, 141, and 113 mAh g^{-1}, respectively, which corresponds to 6.9, 2.6, and 1.0 ions per ZTC "supercage" (a rough estimation of the primary cavity within the pore network of ZTC, connected by four 12 Å pore entrances). Such cells were possible to cycle

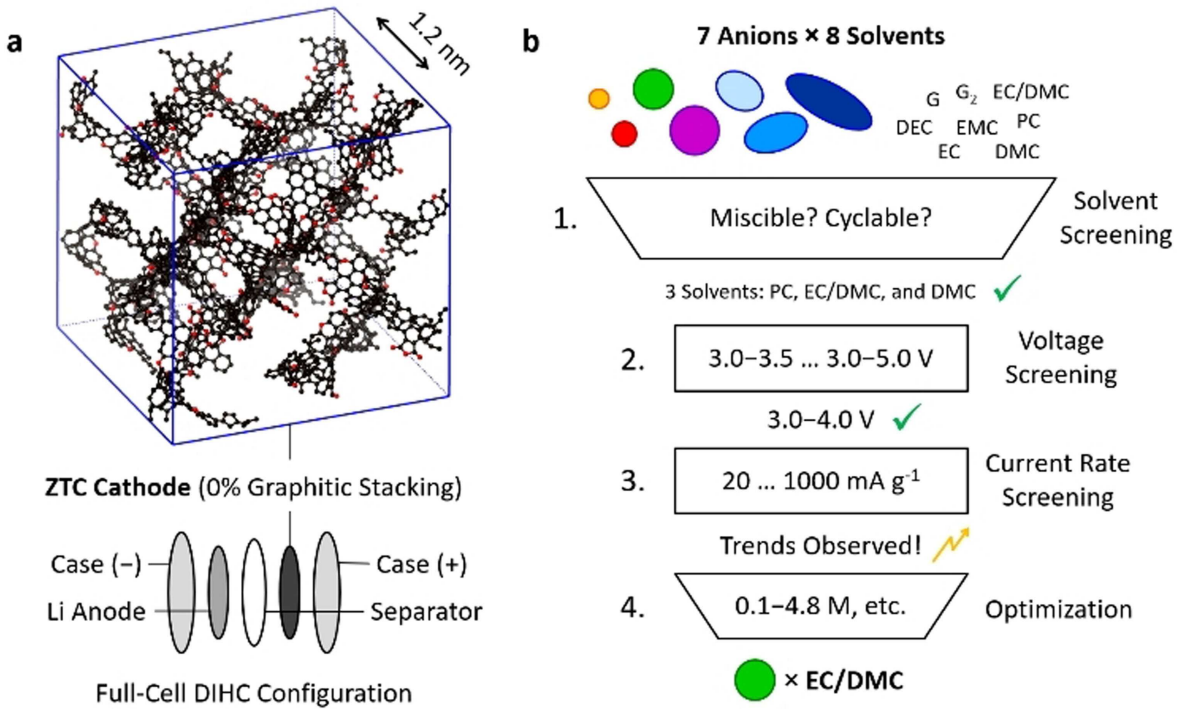

Figure 1. (a) Atomistic structural model of FAU-ZTC (Nishihara Model II+[20]), showing extremely high porosity (≈80%) and no graphitic stacking, and the corresponding DIHC full-cell configuration. (b) Experimental protocol showing the field of anions and solvents screened herein, and subsequent down-selection of solvents and conditions for determining trends in capacitive ion storage in ZTC, leading to the final optimization of one anion/solvent pair.

between 2.43, 3.60, and 2.01 V, all vs. Li/Li^+, respectively, permitting relatively high voltages and therefore high energy densities, both gravimetrically and volumetrically. The differences in ion size cannot account for the different ultimate capacities within each chemistry. Furthermore, none of these capacities seems to have reached the maximum packing density of ions into the ZTC pore space, indicating that solvent is co-inserting along with the relevant ions during charge/discharge cycling. It is also clear that the type of solvent significantly effects the maximum ion capacity of ZTC.

Guiding principles for how to design DIBs and DIHCs where the solvent co-inserts with the anion of interest in the porous carbon electrode are needed. In this work, the solvent, anion, and electrochemical conditions are methodologically varied to understand the roles of ion shape and size, solvent shape and size, and viscosity and ionic conductivity of the electrolyte. Lithium was chosen as the counter ion for simplicity and was not the focus of this study. A series of carbonate solvents was chosen since this type of solvent has the greatest issues associated with anion co-insertion. A simple protocol for down-selection of the electrolyte composition and voltage range of study was conceived, as shown in Figure 1b. Based on this approach, trends could be determined and used to draw conclusions regarding the optimal electrolyte to achieve high ion inclusion within the ZTC structure at different current rates and voltage windows. The optimal electrolyte for high power density was then optimized to demonstrate the utility of this approach in achieving useful cell formulations for applications.

Results and Discussion

Dual-ion electrochemistry

In a porous carbon/metal DIHC, the anion is inserted within the porous carbon positive electrode upon charge (while the cation plates at the bare metal negative electrode) and the opposite upon discharge. Hence, half-cell chemistry is the same as full-cell chemistry since the intended full-cell contains the bare metal as the negative electrode. The focus of the present study is to investigate insertion/deinsertion within the porous carbon framework, and interrogate the effects of anion size, solvent molecular size, and solvent properties on reversible storage capacity and rate capability. A purely microporous (12 Å pore width, without any graphitic stacking) carbon cathode material (ZTC) was used without any binder or additive (the effects of a polytetrafluoroethylene (PTFE) binder are shown in the Supporting Information). All studies were performed with Li metal as the negative electrode, and hence Li^+ as the counterion. Upon charging, the relevant reactions are as follows [Eqs. (1) and (2)]:

$$\text{Negative electrode}: \ Li^+ + e^- \rightarrow Li \tag{1}$$

$$\text{Positive electrode (ZTC)}: \ x\ C + A^- \rightarrow [A]C_x + e^- \tag{2}$$

The charging process ends when either all of the Li^+ cations or all of the relevant anions are depleted in the electrolyte (and therefore plated at the negative electrode or stored within the pore network of ZTC) or when the ZTC reaches its maximum anion storage capacity. A large excess of electrolyte is used in this work to prevent the former scenario. Contrary to LIBs, the open-circuit voltage (OCV) of a DIHC depends on the electrolyte and the chemical potentials of its substituents, as described by the Nernst equation [Eq. (3)]:

$$-eV = \mu^{\circ}_{Li} + \mu^{\circ}_{A} - \mu^{\circ}_{Li^+} - \mu^{\circ}_{A^-} - 2\ k_B T \ln[Li^+] \tag{3}$$

In this equation, $\mu^{\circ}_{Li^+}$ and $\mu^{\circ}_{A^-}$ are the chemical potentials of the cation and anion in solution, μ°_{Li} is the chemical potential of the Li atoms in the metal, and μ°_{A} is the chemical potential of the anions inserted into ZTC upon charging.[7] This means that the OCV of a DIHC will depend on the identity of both the anion and the solvent. The OCV of the cell compositions explored in this work varied between 2.8–3.4 V vs. Li/Li^+ (see Tables S2, S3).

Electrochemical protocols

The electrochemical focus of this research is two-fold: to establish common reversibility limits with respect to the electrochemical stability window of ZTC within a diverse assortment of electrolytes and, thereafter, to study the effects that anion and solvent properties have on capacity and current rate within a stable cycling regime. Stepwise opening of the potential window of charge/discharge cycling (in 5 cycle intervals) as well as cyclic voltammetry revealed the extent of oxidation at the ZTC electrode and other side reactions. Based on this information, an appropriate window was chosen for further current rate dependency experiments within the range of 20 to 1000 $mA\,g^{-1}$. This method of down-selection of electrolyte compositions and operation parameters is shown schematically in Figure 1b.

Three solvents [dimethyl carbonate (DMC), ethylene carbonate (EC)/DMC, and propylene carbonate (PC)] and seven different anions [ClO_4^-, BF_4^-, PF_6^-, SbF_6^-, FSI^-, $FTFSI^-$, and $TFSI^-$ (FSI = bis(fluorosulfonyl)imide], a total of 21 electrolytes, were studied. Solvents composed of DEC, glyme, and diglyme either never achieved a capacity above 1 $mAh\,g^{-1}$ or became too viscous to operate at the desired 1 M concentration and were therefore disregarded. The anions consist of two distinct types: spherical oxo- or fluoro-anions (ClO_4^-, BF_4^-, PF_6^-, and SbF_6^-) and spheroidal fluorosulfonylimide anions (FSI^-, $FTFSI^-$, and $TFSI^-$). Perchlorate, ClO_4^-, while spherical, is an outlier within that series due to its low oxidative stability/potential and high highest occupied molecular orbital (HOMO) energy.[33]

Potential window studies

To achieve cycling stability in a DIHC, the cathodic and anodic potentials must be between the HOMO and lowest unoccupied molecular orbital (LUMO) of the electrolyte.[34] If the Fermi level of the cathode is located below the HOMO of the electrolyte, oxidation of the electrolyte occurs [unless the reaction is

blocked by an solid electrolyte interphase (SEI) layer]. On the other hand, if the Fermi level of the anode is located above the LUMO of the electrolyte, then the electrolyte will be reduced. The SEI layer, though mainly formed in the first charge cycle, continues to thicken in each subsequent charge cycle; as this decomposition occurs, Li^+ cations, anions, and solvent are depleted, one potential cause of capacity fading.[35] The OCV is the difference between the Fermi levels of the electrodes and, in order to maximize the energy density of a cell, this difference must be maximized without exceeding the window afforded by the electrolyte stability. The anion often sets the oxidation limit of the electrolyte[33] whereas solvent properties (dielectric constant, molecular size, viscosity, etc.) play an important role in ionic conductivity.[36,37]

To establish the stable potential window for later rate capability tests, each cell was cycled 40 times at the benchmark current rate established in previous work (100 mA g^{-1}),[24] widening the voltage window every 5 cycles, thereby exploring 8 different voltage ranges of interest (from 3.0–3.5 to 3.0–5.0 V vs. Li/Li^+). In this way, the voltage limit beyond which degradation occurs due to oxidative side reactions at the ZTC electrode could be identified. The results for all anions in EC/DMC are shown in Figure 2a, and representative results for PF_6^- in EC/DMC are shown in Figure 2b. In $LiPF_6$ in EC/DMC, ZTC showed a steady increase in discharge capacity with increasing maximum voltage, up to the widest potential window explored (3.0–5.0 V). This electrolyte showed five consecutive cycles of coulombic efficiencies exceeding 90% up to the 3.0–4.2 V potential window (Figure 2a). A plateauing feature at the top of the charge step in a voltage profile indicates decomposition of the electrolyte; for example, 1 M $LiPF_6$ in EC/DMC begins to show such decomposition at $>$4.2 V vs. Li/Li^+ (Figure 2c).

Across all of the 21 electrolyte combinations explored in stepwise potential opening studies, between 0.1–0.6 anions could be reversibly inserted into each ZTC supercage (defined as described in the Supporting Information) within the 3.0–4.0 V range, suggesting that general conclusions could be made about the role of anion size/shape and solvent molecular size/character on current rate dependencies in that range (Figure S1a–c). Therefore, the 3.0–4.0 V voltage window was chosen for further trend analysis due to consistent coulombic efficiencies above 90%. Higher capacities within wider overall voltage windows were observed for $LiPF_6$ in EC/DMC and therefore that system was later chosen for further optimization.

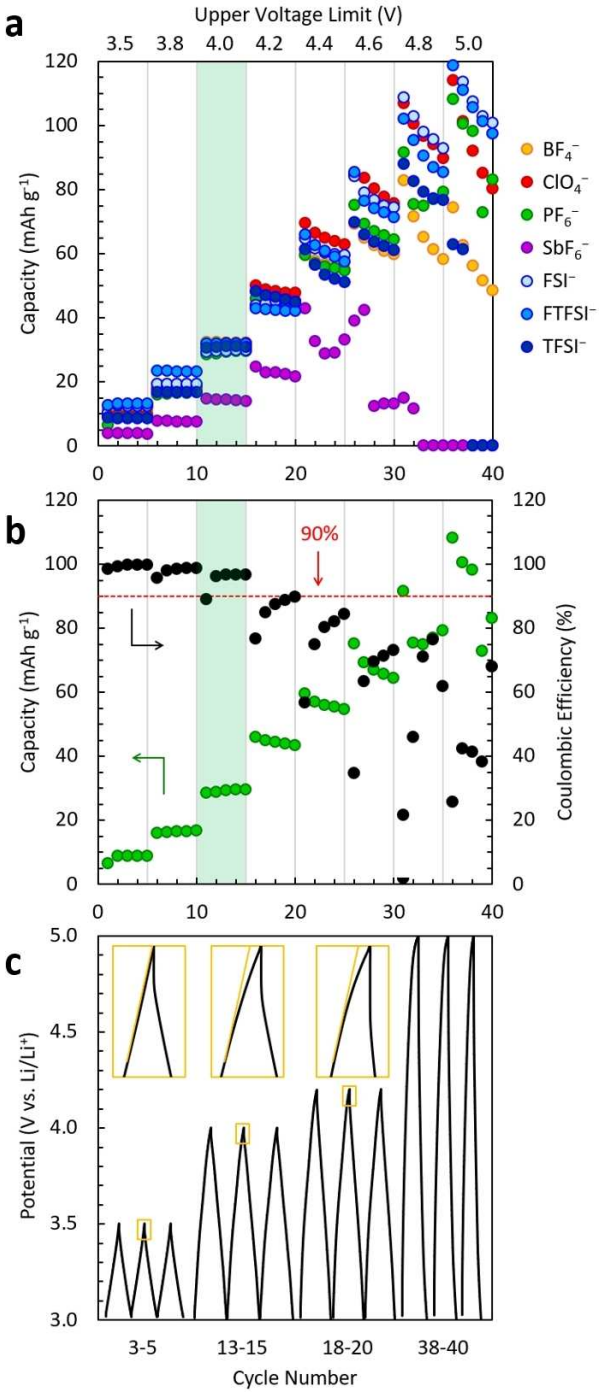

Figure 2. Voltage opening electrochemical characterization of ZTC DIHCs cycled at 100 mA g^{-1}. (a) Potential window screening (3.0–3.5…5.0 V) of all anions in EC/DMC, showing discharge capacity (colored symbols) at 100 mA g^{-1}. (b) Representative potential window screening for PF_6^- in EC/DMC, showing discharge capacity (green symbols) and coulombic efficiency (black symbols) at 100 mA g^{-1}. (c) Representative three-cycle galvanostatic charge/discharge profiles for PF_6^- in EC/DMC between: 3.0–3.5, 3.0–4.0, 3.0–4.6, and 3.0–5.0 V, as a function of cycle number.

Current rate studies

A wide range of electrolyte compositions were explored to determine the role of the previously mentioned electrolyte properties on specific capacity at current rates up to 1 A g^{-1}. Cells containing each of the 21 electrolyte combinations (at 1 M concentration) were subjected to an increasing current rate protocol (20, 50, 100, 200, 500, and 1000 mA g^{-1}) within the aforementioned common voltage window of 3.0–4.0 V vs. Li/Li^+ (Figure S2a–c). As expected, the capacities of all cells were inversely correlated with current rate. The experimental results reveal that anion/solvent size and solvent viscosity/dielectrics have subtle but important effects on specific capacity, current rate dependence, and voltage window stability. The structural

and electrochemical properties of the anions and solvents used are shown in Table 1, and a summary of the results of the broad electrochemical screening experiments is presented in Figure 3. A discussion of some of the important trends in these data is given in the next several sections.

Anion size effects

At low current rates, equilibrium is effectively reached and the maximum number of anions are stored, regardless of the electrolyte composition. Accordingly, the maximum reversible capacity generally decreases as a function of anion volume at 20 mA g^{-1} (Figure 3, black series). The smallest anion studied, BF_4^-, exhibits the highest capacity in the screening tests (35 mAh g^{-1}, or 0.63 anions per supercage, in PC). Likewise, the largest anion studied, $TFSI^-$, exhibits the lowest capacity (25 mAh g^{-1}, or 0.46 anions per supercage, in PC). The maximum capacities at each current rate among the different anions are surprisingly similar. Hence, the overall volume occupied by the anions within the ZTC supercages is higher for the larger anions; this indicates that occupancy within the pores is less limited by a "pore filling" mechanism and rather more limited by a "monolayer adsorption" mechanism (i.e., limited by a fixed

Table 1. Structural and electrochemical properties of anions in this study.

Type	Anion	Volume [Å^3]	Narrowest width [Å]	Length [Å]	Diameter[a] [Å]	OS[b][33] [V vs. Li/Li$^+$]	OS[b][38] [V vs. Li/Li$^+$]
spherical	BF_4^-	73	5.61	5.66	5.19	6.35	6.01
	ClO_4^-	82	5.87	5.90	5.39	4.36	3.87
	PF_6^-	103	6.59	6.60	5.82	8.57	6.51
	SbF_6^-	124	7.06	7.12	6.19	NR[c]	NR
spheroidal	FSI^-	150	5.83	8.40	6.59	5.34	4.19
	$FTFSI^-$	198	7.11	9.43	7.23	NR	NR
	$TFSI^-$	245	7.12	10.34	7.76	6.12	4.48

[a] Diameter of a sphere with the same volume. [b] Oxidative stability. [c] NR: not reported.

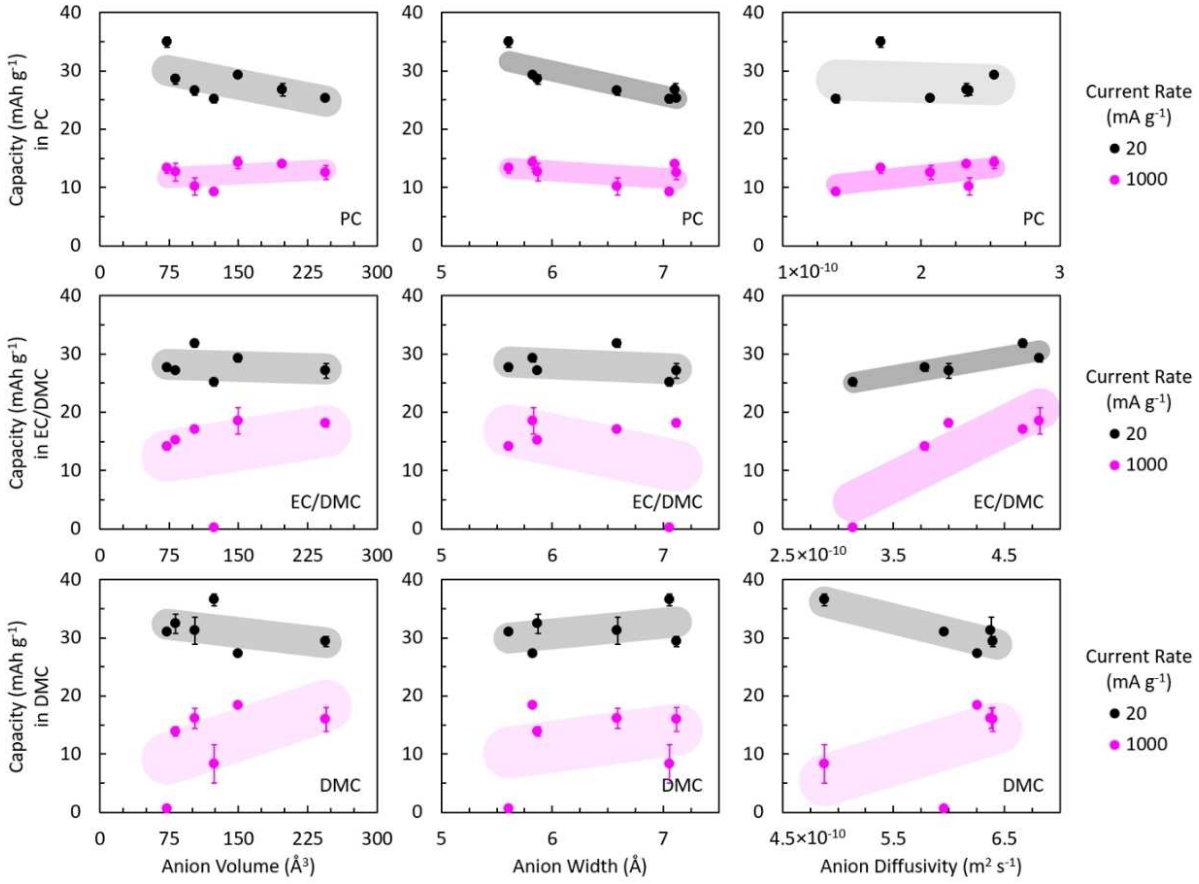

Figure 3. Anion storage capacity in ZTC as a function of anion volume, narrowest width, and diffusivity, from reversible discharge capacity between 3.0–4.0 V vs. Li/Li$^+$. Low current rate data (20 mA g^{-1}) are shown in black and high current rate data (1 A g^{-1}) are shown in pink. Stronger correlations are indicated by heavier and narrower (linear) trend lines, as a guide for the eye. Error bars are across measurements in triplicate or more.

number of adsorption sites) and strongly reveals solvated anion insertion. The narrowest width is typically more correlated to capacity than the anion volume, which also indicates a "monolayer adsorption" type model as opposed to "pore filling." At high current rates (Figure 3, pink series), anion size shows significantly less correlation (except in PC, where the capacity is effectively the same for all anions) and capacity is therefore better attributed to other factors.

Anion diffusion effects

The diffusivity of each anion in each solvent was measured using pulsed-field gradient nuclear magnetic resonance (NMR) spectroscopy (see Table 2). Efforts to perform ^{35}Cl NMR spectroscopy were unsuccessful, and therefore ClO_4^- was excluded from this comparison. In general, anion diffusivity was inversely correlated with both viscosity and dielectric constant among the three solvents explored (see Figure S3). Hence, diffusivity was found to be more significantly a property of the solvent rather than the anion. Since diffusivity is expected to play an important role at high current rates, the capacity of all anions as a function of diffusivity at the maximum current rate explored (1 A g^{-1}) is shown in Figure 4.

The spherically shaped anions did not show a correlation between diffusivity and width in any solvent, which suggests that the higher electronegativity of phosphorous played a key role in its diffusivity (see Figure 4a). In EC/DMC and PC, the spheroidal shaped ions showed a negative correlation between diffusivity and width. The solvent that gave rise to the largest differences in diffusivity of the anions (within the same solvent) was EC/DMC, and this solvent system is therefore best representative of anion diffusivity effects. In EC/DMC, there is a strong correlation between diffusivity and capacity, as shown in Figure 3. This is consistent with the general trend observed for all solvent systems in Figure 4, thus confirming the importance of anion diffusivity for high current rate storage within the nanometer-sized channels of ZTC.

In EC/DMC, the cations and anions are more closely paired and therefore diffusion takes priority over anion size in determining anion capacity.

Solvent size effects

The three solvents chosen for analysis in this study also display a range of physicochemical properties, permitting an assessment of the role of the solvent in anion storage in ZTC-based DIHCs. Anion capacity as a function of solvent molecular size is shown across all anions in Figure 5. It is clear that solvent molecular size is not the main dictating property of anion capacity in ZTC, neither at low nor at high current rates. Solvation structure influences several aspects of anion insertion, including diffusion as well as volume and shape occupied by the anion within the ZTC pores; the identity of the solvent also affects the structure of the passivation layer formed at the electrode interface (cathodic electrolyte interphase, CEI).[14,37] Solvents with a high dielectric constant provide good solubility of the electrolyte salt, but also bring about high viscosity which slows ion transport. Solvents with a low dielectric constant provide fast ion transport but also increased ion-pairing effects between Li^+ and the anion due to their low solubility.[13] Therefore, solvent mixtures comprising components with different individual properties are often chosen to provide an effective compromise within this trade-off. A more detailed comparison of the properties of the three solvents chosen in this work is given in Table S5.

Table 2. Anion diffusivity (in 10^{-10} m^2 s^{-1}) in each of the solvents in this study: DMC, EC/DMC, and PC.

Type	Anion	DMC	EC/DMC	PC
spherical	BF_4^-	5.96	3.79	1.71
	PF_6^-	6.38	4.67	2.35
	SbF_6^-	4.88	3.14	1.39
spheroidal	FSI^-	6.26	4.82	2.53
	$FTFSI^-$	6.43	4.48	2.33
	$TFSI^-$	6.40	4.00	2.07

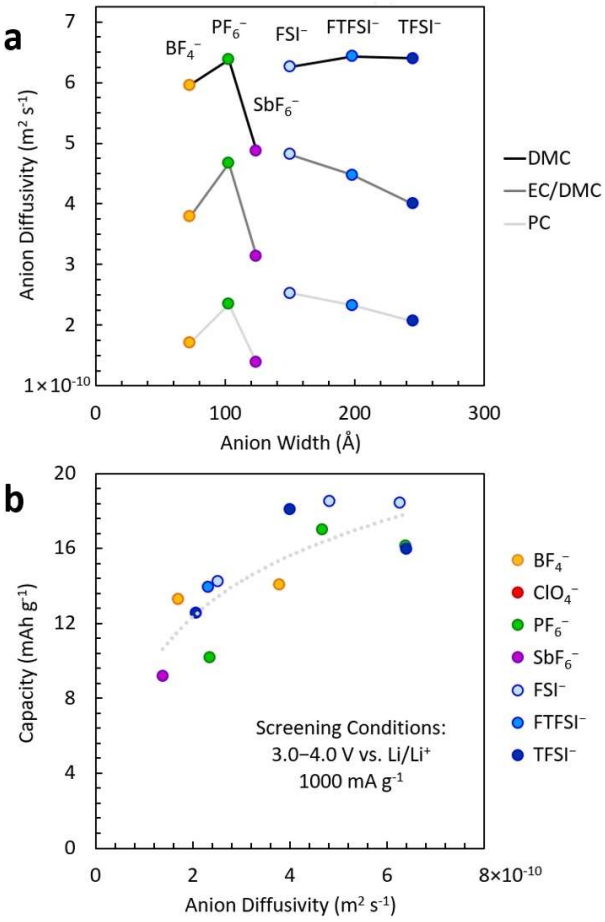

Figure 4. (a) Anion diffusivity as a function of anion volume in each of the solvents in this study: DMC, EC/DMC, and PC. (b) Anion storage capacity in ZTC as a function of anion diffusivity across all solvents, from reversible discharge capacity at 1 A g^{-1} between 3.0–4.0 V vs. Li/Li^+.

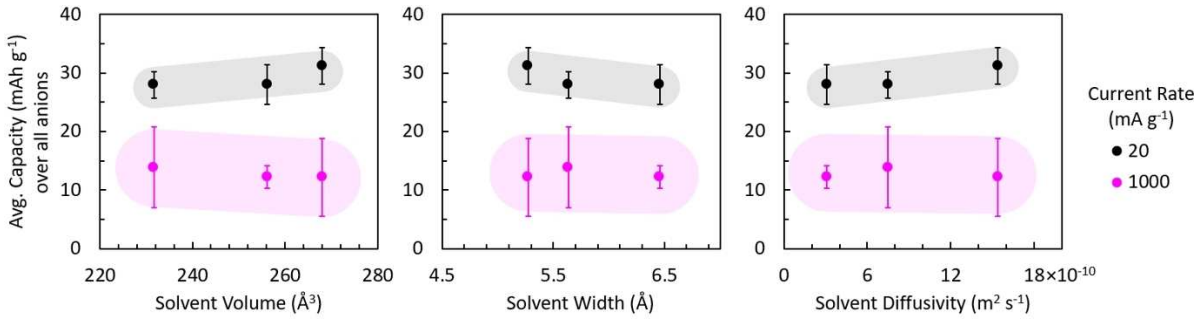

Figure 5. Average anion storage capacity in ZTC as a function of solvent diameter, narrowest width, and diffusivity from reversible discharge capacity between 3.0–4.0 V vs. Li/Li$^+$. Low current rate data (20 mA g^{-1}) are shown in black and high current rate data (1 A g^{-1}) are shown in pink. Error bars are standard deviations across all anions, tested in triplicate.

Solvation structure effects

To better understand the complex role of solvation structure on anion capacity in ZTC, the smallest (BF_4^-) and the largest ($TFSI^-$) anions were chosen for further analysis (Figure 6). It has been shown that the binding energy of the Li–BF_4 pair is slightly higher than the Li–TFSI pair, with binding distances of 1.91 and 2.00 Å, respectively.[39] At low current rates, smaller and more electronegative anions such as BF_4^- benefit from a highly polar solvent that reduces ion pairing. For example, the highest capacity reported in this work's initial screening studies (32.5 mAh g^{-1}, at 20 mA g^{-1}) corresponds to the storage of BF_4^- solvated by PC. On the other hand, large anions such as $TFSI^-$ dissociate more readily due the more delocalized charge over the entire molecule. Hence, $TFSI^-$ benefits from a low viscosity solvent that enhances ion mobility, even at low current rates. At high current rates, both BF_4^- and $TFSI^-$ show their highest capacities in EC/DMC, suggesting that the high dielectric

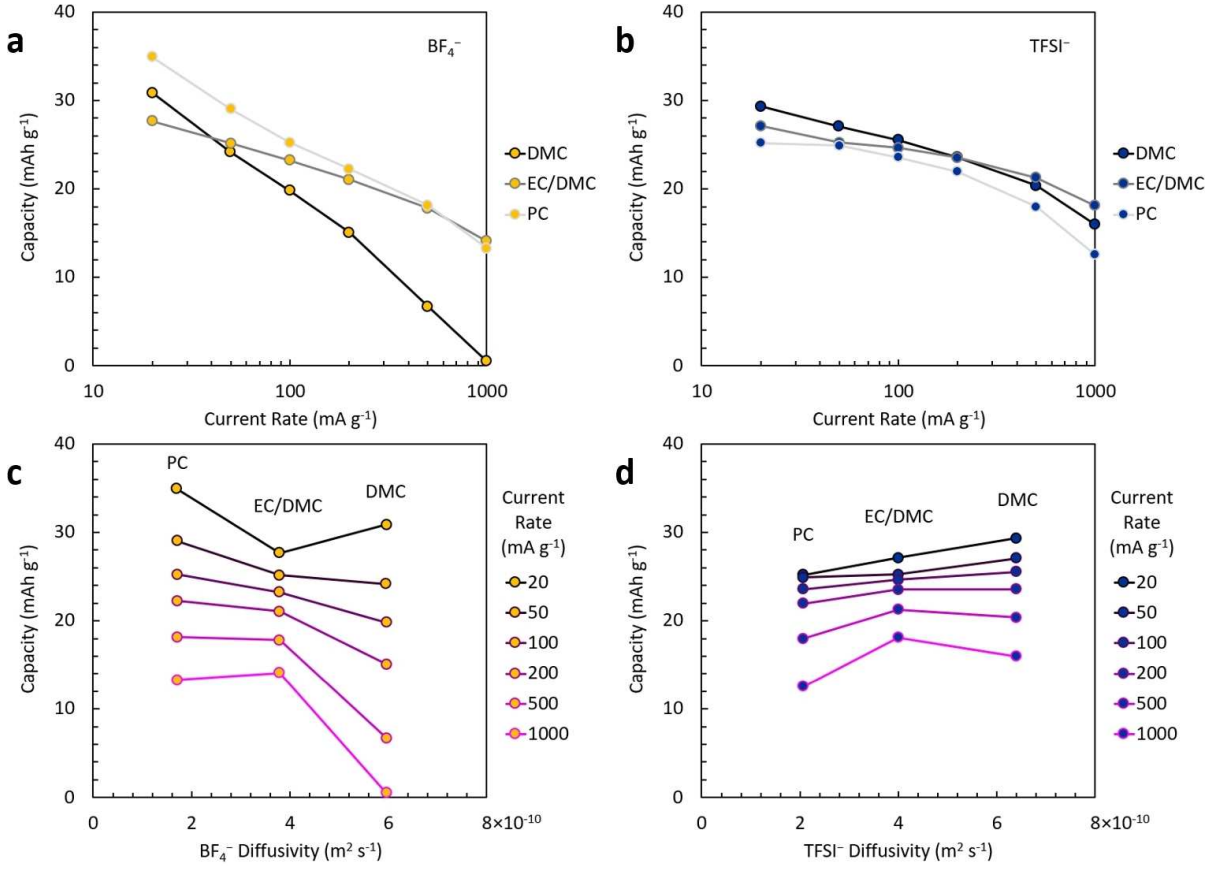

Figure 6. Anion storage capacity as a function of (a,b) current rate [mA g^{-1}] and (c,d) anion diffusivity, for (a,c) BF_4^- and (b,d) $TFSI^-$ cycled between 3.0–4.0 V vs. Li/Li$^+$.

constant of EC and the low viscosity of DMC permit a synergy of properties accommodating both types of anions. It is possible that anions in EC/DMC preferentially insert under solvation by EC (leaving the DMC molecules in solution), serving to maintain a low viscosity (high ion mobility) electrolyte; further studies are warranted to assess the role of stored ion solvation in binary solvent electrolytes. Nevertheless, the results obtained herein generally support the strategy of employing a binary solvent system to exploit the trade-off between solubility and ion mobility.[13,38]

Optimization studies

The screening studies across many electrolyte compositions were performed in the common stability range of 3.0–4.0 V vs. Li/Li^+ and with 1 M nominal concentrations to permit a controlled analysis of the effects of anion and solvent properties. In these experiments, less than 1 anion per ZTC supercage was observed to be inserted even at the slowest current rates explored, far lower than the maximum expectable capacity on the basis of complete pore filling by bare anions. For example, we estimate that 2.7 PF_6^- ions per supercage can be inserted into the pore volume of ZTC (probe accessible volume per unit cell: 17605 Å^3, total volume per unit cell: 111563 Å^3, for Nishihara Model II+). While such estimates do not consider the role of solvent nor the effect of anion-anion repulsion, they indicate that higher capacities would be achievable under optimized conditions.

Owing to its high capacity at low current rates, good oxidative stability at >4.0 V vs. Li/Li^+, and admirable rate capability at up to 1 A g^{-1}, further optimization studies were focused on PF_6^- in EC/DMC as the model electrolyte. Cyclic voltammetry was first performed within incrementally increasing potential windows to establish the maximum stable window in which electrolyte and/or ZTC decomposition could be avoided. This window was determined to be between 2.5–4.6 V vs. Li/Li^+ (Figure S4). A concentration series was analyzed that consisted of 0.1, 1.0, 2.0, 3.0, and 4.8 M electrolyte solutions. In this study, a maximum capacity of 128.9 mAh g^{-1} was achieved between 2.5–4.6 V vs. Li/Li^+ in 3.0 M $LiPF_6$ in EC/DMC at 100 mA g^{-1}, corresponding to around 2.3 anions per ZTC supercage (Figure 7). This is slightly shy of the theoretical limit described above, which suggests that further optimization could perhaps improve capacity.

Several effects on the anion capacity can be observed upon varying the concentration of the electrolyte. The concentration of $LiPF_6$ in EC/DMC was positively correlated to discharge

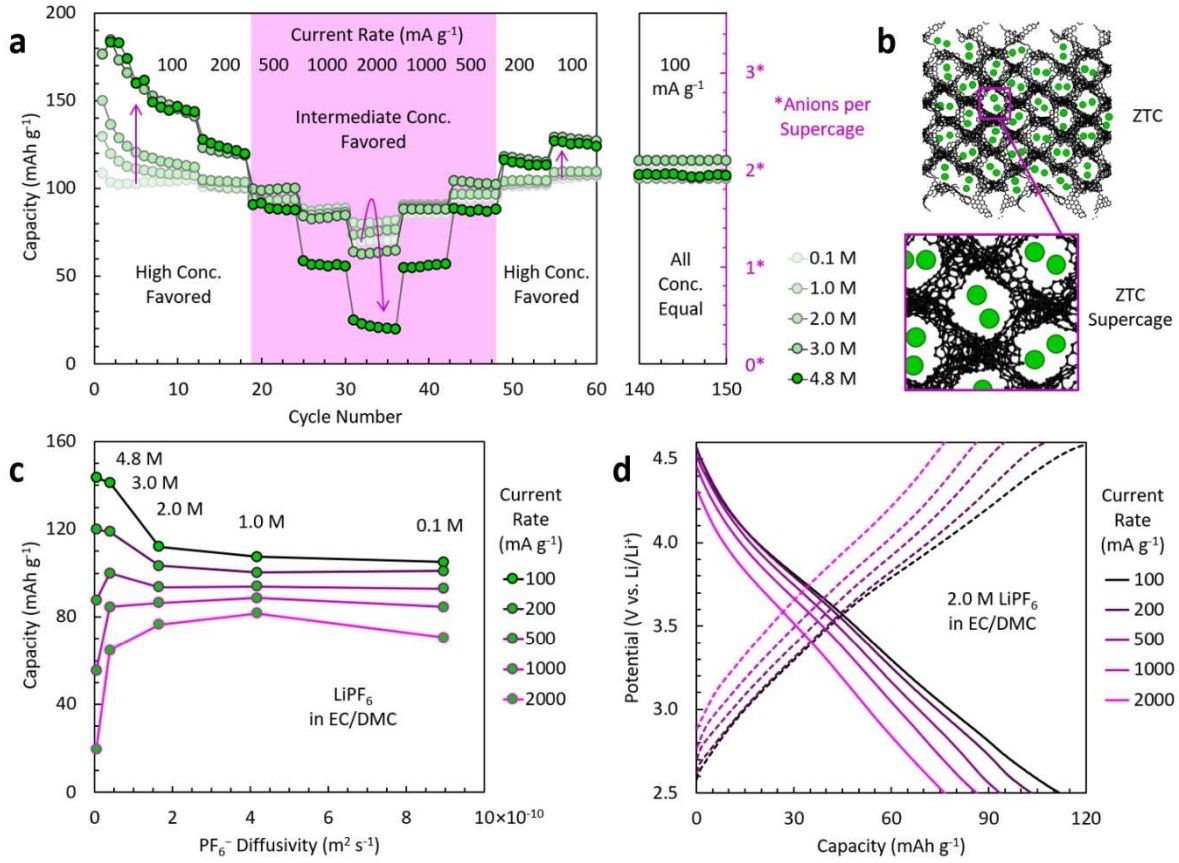

Figure 7. Concentration series of PF_6^- in EC/DMC cycled from 2.5–4.6 V vs. Li/Li^+ and from 100 to 2000 mA g^{-1} in units of (a) discharge capacity [mAh g^{-1}] and/or ions per supercage as a function of cycle number and (c) discharge capacity as a function of diffusion coefficient (in 10^{-10} m^2 s^{-1}). (b) Schematic depiction of long-cycling anion capacity of PF_6^- in ZTC and (d) representative voltage profiles for 2.0 M $LiPF_6$ in EC/DMC. Note: the concentration is given as the nominal (initial) concentration prior to dissolution.

capacity at low current rates, but negatively correlated at high current rates for all concentrations except 0.1 M (Figure 7a). In other words, while high concentration (e.g., 4.8 M) improves capacity at low current rates, the capacity is subject to extreme reduction upon increasing the current rate, an effect that can be attributed to increased viscosity and slow diffusion. The diffusivity as measured by pulsed-field gradient stimulated echo (PFGSTE) NMR experiments corroborates this explanation (as shown by the pink trace for 2 A g^{-1} in Figure 7c). Evidence for increased ion pairing with concentration is also observed in that the Li^+ and PF_6^- diffusion rates converge at high concentrations. The slightly higher deviation of the capacities at 0.1 M compared to 1.0 M can be attributed to a decrease in ionic conductivity caused by a low concentration of charge carries, even though the diffusivity is the highest.

Cyclic voltammetry and Randles–Ševčík analysis of PF_6^- storage within ZTC showed exclusively capacitive behavior within the common stability window chosen for comparison to all other anions (3.0–4.0 V vs. Li/Li^+). Upon widening the voltage window to between 2.5–4.6 V vs. Li/Li^+, charge storage adopted a more Faradaic character (Figure S6), suggesting that the anions are adsorbed within more confined regions of the ZTC supercages that encourage more charge transfer than when stored under lower density conditions. Self-discharge analysis revealed that some leakage occurs even from within these confined regions of the ZTC pores (Figure S10), a common issue facing DIHC electrodes. Interestingly, after 100 cycles at 100 mA^{-1}, electrolytes of all concentrations explored converged on the same capacity of around 110 mAh g^{-1} or around 2.0 ions per supercage. This indicates a seeming equilibrium capacity of ZTC toward PF_6^- that is reversible across a wide range of electrolyte compositions at the benchmark current rate. To better understand this capacity, a comparison can be drawn to PF_6^- storage in graphite; the maximum intercalation capacity in graphite corresponds to a stage-1 compound of composition PF_6C_{24}.[12,13] Hence, in graphite, the minimum in-plane PF_6–PF_6 distance is around 8.5 Å. In ZTC, this distance is reduced to (on average) around 6 Å given the accessible pore width of 12 Å. Likewise, the composition is slightly more enriched with anions on a per-carbon basis, corresponding to a maximum of around PF_6C_{18} for ZTC (without regard for the hydrogen or oxygen content). Nevertheless, it is expectable that anion–anion repulsion, in addition to steric hindrance of the included solvent, is responsible for determining the maximum upper capacity within the ZTC framework.[40]

Conclusions

Zeolite-templated carbon (ZTC) serves as an ideal model material for understanding the mechanism of anion storage in nanometer-sized carbon pore spaces because of its ordered framework of 1.2 nm pores that is robust to charge and discharge at potentials relevant to use as a positive electrode in dual-ion hybrid capacitors (DIHCs). The methodological variation of anions and solvents has been employed herein to elucidate guiding principles for the roles of anion and solvent molecular size, shape, and other properties (such as diffusivity) on storage capacity, at both the low and high current rate extremes. Full-cells based on a ZTC cathode and electroplating/stripping of lithium metal at the negative electrode demonstrate specific energies of 146 Wh kg^{-1} and power densities of >4000 W kg^{-1}, which are realistic values for studying the effects of electrolyte properties. Solvation structure upon charging is difficult to study due to the rigid nature of ZTC and therefore future work analyzing binary and tertiary solvent systems will help to understand the effects of ion pairing. Electrolyte composition is a key part of battery and capacitor design and the fundamental understanding of how these molecules interact within such systems provides insights towards optimization.

Experimental Section

Materials synthesis

ZTC was prepared according to the established two-step method,[26,27] via liquid impregnation of zeolite NaY with furfuryl alcohol at room temperature and then chemical vapor deposition of propylene at 700 °C; after heat treatment at 900 °C, the zeolite template was removed upon repeated dissolution in aqueous HF. The synthesis methods are described in detail in the Supporting Information.

Materials characterization

Powder X-ray diffraction (XRD) measurements were performed using a Bruker D8 Advance diffractometer with Cu $K_{\alpha 1,2}$ radiation ($\lambda = 1.54$ Å) in reflection geometry. Nitrogen adsorption/desorption isotherms were measured at 77 K between 10^{-4}–100 kPa using an automated volumetric instrument (3Flex, Micromeritics Instrument Corp.). Specific surface areas were calculated by the Brunauer-Emmett-Teller (BET) method between $P/P_0 = 4\times10^{-6}$–0.11 and micropore volumes were calculated by the Dubinin-Radushkevich (DR) method.[28] Pore-size distributions were determined by non-localized density functional theory (NLDFT) calculations with a carbon slit-pore model (using MicroActive Share software, Micromeritics Instrument Corp.).

Electrochemical cell materials

The following materials were used in the preparation of electrochemical cells: ethylene carbonate (EC, battery grade, BASF), dimethyl carbonate (DMC, battery grade, BASF), propylene carbonate (PC, 99.7 %, Sigma Aldrich), lithium perchlorate ($LiClO_4$, 99,9 %, ABCR), lithium tetrafluoroborate ($LiBF_4$, 99 %, Acros), lithium hexafluorophosphate ($LiPF_6$, 99 %, Novolyte), lithium hexafluoroantimonate ($LiSbF_6$, 99 %, Apollo), lithium bis(fluorosulfonyl)imide (LiFSI, 99 %, Henan Tianfu Chemical Co.), lithium (fluorosulfonyl)(trifluoromethanesulfonyl)imide (LiFTFSI, 99.7 %, Provisco), lithium bis(trifluoromethanesulfonyl)imide (LiTFSI, 99 %, Acros), lithium foil (Li, 99 %, Fluka), and glass microfiber discs (0.67 × 257 mm, GF/D grade, 1823–257, Whatman).

Electrolyte preparation

The electrolyte was prepared by slowly mixing the given lithium salt/solvent combinations at the specified concentrations (see the

Supporting Information, Tables S1, S2) under inert Ar atmosphere (< 0.1 ppm H_2O/O_2). A dual solvent electrolyte (EC/DMC) was prepared at a 1:1 ratio, by weight. In all cases, an exothermic reaction takes place upon dissolution of the salt, resulting in the eventual formation of a viscous, transparent liquid. The electrolyte concentration reported is the nominal concentration based on the initial volume of the solvent, not the final volume. The actual (final) concentrations corresponding to each nominal concentration in the $LiPF_6$ in EC/DMC series are shown in Table S2.

Current collector coating

To improve cycling stability under high-voltage conditions, the stainless-steel coin cell caps (316L, 2032 size, Hohsen Corp.) were coated at the positive electrode side with TiN by pulsed DC magnetron sputtering using a titanium target under a flowing Ar/N_2 atmosphere at a pressure of 0.5 Pa, as previously described.[29,30] The sides of the current collectors, parallel to the sputtering beam and thus less coated by TiN, were further protected with a thin layer of epoxy glue (Araldite Rapid).

Electrochemical cell preparation

Stainless-steel coin cells were assembled in a glovebox under inert Ar atmosphere (< 0.1 ppm H_2O/O_2). The active electrode material (ZTC), simply as a dry, activated powder, was homogeneously dispersed on the TiN-coated stainless-steel cap. In general, the use of a binder results in poorer accessibility of the porous electrode; these effects are described in the Supporting Information. A single glass microfiber disc was then placed on top of the bare ZTC powder as the separator, and saturated with 250 μL electrolyte. A thin lithium film (≈60 mg) pressed onto a stainless-steel disc was placed on top of the separator and was used as both the reference and counter electrodes. A stainless-steel spring and cell bottom were placed on top of the reference electrode and compressed with a hydraulic press. The working electrode was prepared as a loose powder without the use of any binder, conductive additive, or solvent, and the electrolyte was used as prepared above. Each cell contained a 0.9–1.3 mg loading of active cathode material (ZTC).

Electrochemical measurements

Before galvanostatic cycling, the prepared cells were held at OCV for 2 h to allow the ZTC electrode to become fully wetted with electrolyte. The OCV of the cells was between 2.8–3.4 V vs. Li/Li^+. Galvanostatic cycling was performed using a multi-channel workstation (CT2001A, 0.005–1 mA, Landt Corp.). The measured specific discharge capacity (number of ions deinserted) was normalized by the total initial mass of the active material (since no binder or conductive additive were used). Cyclic voltammetry was performed using a separate multi-channel workstation (MPG-2, BioLogic SAS).

NMR spectroscopy

The diffusivity and ionic conductivity of each species in each electrolyte was determined using multinuclear (^1H, ^7Li, and ^{19}F) NMR spectroscopy. A 200 μL aliquot of each as-prepared electrolyte was subjected to a PFGSTE pulse sequence using a 500 MHz NMR spectrometer (Ascend 500, Bruker Corp.) equipped with an Avance III HD console (Bruker Corp.), an automatic sample loading system (SampleJet, Bruker Corp.), and a 5 mm liquid nitrogen-cooled broadband (BBO) cryoprobe (Prodigy, Bruker Corp.). Spectra were acquired using the ledbpgp2 s pulse sequence (Bruker Corp.), and t2×t1 matrices of 16384×20 points (for ^1H) or 131072×20 points (for ^7Li and ^{19}F) were collected. The *z*-axis gradient strength varied linearly from 2 to 98% of its maximum value (65.7 G cm^{-1}), the gradient pulse duration was 2.8 ms (for ^1H and ^{19}F) or 4.8 ms (for ^7Li), and the time period between the two gradient pulses was 50 ms (for ^1H and ^{19}F) or 100 ms (^7Li). The relaxation delay (D1) ranged between 3–10 s. All measurements were performed at a constant temperature of 300 K and the results were analyzed using a dedicated software package (Topspin v3.6, Bruker Corp.). Self-diffusion coefficients (referred to herein as diffusivity, D) were determined by fitting the NMR intensity as a function of time to the Stejskal-Tanner equation.[41]

Anion capacity metrics

Reversible charge/discharge capacity [mAh g^{-1}] was converted into "number of ions per supercage" of the ZTC framework on the basis of the number of "supercages" per unit mass of ZTC. The number of ZTC supercages per gram was determined based on a periodic model of ZTC referred to herein as Nishihara Model II+;[21] 64 "supercages" (pore spaces of roughly the same size and shape), corresponding to 64 tetrahedral nodes in the original faujasite (FAU) zeolite template in which it was formed, exist within the cubic unit cell weighing 0.4626 g mL^{-1} (corresponding to a 2×2×2 supercell of unit cells of the faujasite template, $a = 48.14$ Å). An example calculation of ions per supercell, *n*, is given in the Supporting Information. In brief, a capacity of 55 mAh g^{-1} corresponds to 1 anion adsorbed within each supercage of the FAU-ZTC framework.

Computational methods

Theoretical calculations of molecular size and shape were performed using DFT. A global hybrid functional (MN15) together with a triple-zeta basis set (6-311++G**) was chosen based on recent methods employed in our group[31] and general benchmarking studies[32] and implemented using the Gaussian 16 software package. The size of each anion in solution was estimated by optimizing the anion within a polarizable continuum model. To establish the solvent environment for anion calculations, a unique polarizable continuum was generated for each solvent using the solvent radius, dielectric constant, index of refraction, and macroscopic surface tension (see the Supporting Information). Each anion was then optimized in the polarizable continuum, resulting in a solvent excluded surface solvation cavity. The length and width of the solvation cavity were defined as the longest distance between two points on the solvation cavity, and the longest distance between two points perpendicular to the length, respectively. The convex hull of the solvent excluded surface solvation cavity was then calculated to determine the effective volume of each anion. The size of each solvent was estimated by optimizing the solvent molecule alone.

Acknowledgements

We thank Wei Xu for insightful discussions. C.W. and N.P.S. are grateful for funding provided by the National Science Foundation (grant OIA-2034110). P.V., K.V.K., and M.V.K. gratefully acknowledge financial support provided by Empa (internal project "GRAPHION"). We also thank the MSU NMR Center (supported by National Science Foundation grant DBI-1532078 and the M. J. Murdock Charitable Trust grant 2015066:MNL) for access to their

instrumentation and Brian Tripet for assistance in performing the measurements and analysis.

Conflict of Interest

The authors declare no conflict of interest.

Data Availability Statement

The data that support the findings of this study are available in the supplementary material of this article.

Keywords: batteries · electrode materials · energy storage · microporous carbon · supercapacitors

[1] T. Placke, R. Kloepsch, S. Dühnen, M. Winter, *J. Solid State Electrochem.* **2017**, *21*, 1939–1964.
[2] W. H. Li, X. L. Wu, *Electrochem. Sci. Adv.* **2022**, *2*, e2100127.
[3] T. Ishihara, M. Koga, H. Matsumoto, M. Yoshio, *Electrochem. Solid-State Lett.* **2007**, *10*, A74.
[4] J. Xie, Y. C. Lu, *Nat. Commun.* **2020**, *11*, 2499.
[5] T. Panja, J. Ajuria, N. Diez, D. Bhattacharjya, E. Goikolea, D. Carriazo, *Sci. Rep.* **2020**, *10*, 10842.
[6] W. Fan, H. Zhang, H. Wang, X. Zhao, S. Sun, J. Shi, M. Huang, W. Liu, Y. Zheng, P. Li, *RSC Adv.* **2019**, *9*, 32382–32394.
[7] J. A. Seel, J. R. Dahn, *J. Electrochem. Soc.* **2000**, *147*, 892.
[8] T. Placke, O. Fromm, S. F. Lux, P. Bieker, S. Rothermel, H.-W. Meyer, S. Passerini, M. Winter, *J. Electrochem. Soc.* **2012**, *159*, A1755-A1765.
[9] M. Wang, Y. Tang, *Adv. Energy Mater.* **2018**, *8*, 1703320.
[10] J. O. Besenhard, H. P. Fritz, *Angew. Chem. Int. Ed.* **1983**, *22*, 950–975; *Angew. Chem.* **1983**, *95*, 954–980.
[11] H. Zhang, Z. Li, W. Xu, Y. Chen, X. Ji, M. M. Lerner, *Nanotechnology* **2018**, *29*, 325402.
[12] J. A. Read, *J. Phys. Chem. C* **2015**, *119*, 8438–8446.
[13] D. M. Seo, S. Reininger, M. Kutcher, K. Redmond, W. B. Euler, B. L. Lucht, *J. Phys. Chem. C* **2015**, *119*, 14038–14046.
[14] S. Han, *Sci. Rep.* **2019**, *9*, 5555.
[15] Z. Hu, Q. Liu, K. Zhang, L. Zhou, L. Li, M. Chen, Z. Tao, Y. M. Kang, L. Mai, S. L. Chou, J. Chen, S. X. Dou, *ACS Appl. Mater. Interfaces* **2018**, *10*, 35978–35983.
[16] Y. Liang, H. Dong, D. Aurbach, Y. Yao, *Nat. Energy* **2020**, *5*, 646–656.
[17] I. A. Rodríguez-Pérez, X. Ji, *ACS Energy Lett.* **2017**, *2*, 1762–1770.
[18] X. Zhou, Q. Liu, C. Jiang, B. Ji, X. Ji, Y. Tang, H. M. Cheng, *Angew. Chem. Int. Ed.* **2020**, *59*, 3802–3832; *Angew. Chem.* **2020**, *132*, 3830–3861.
[19] T. Placke, P. Bieker, S. F. Lux, O. Fromm, H.-M. Meyer, S. Passerini, M. Winter, *Z. Phys. Chem.* **2012**, *226*, 391–407.
[20] H. Nishihara, T. Kyotani, *Chem. Commun.* **2018**, *54*, 5648–5673.
[21] H. Nishihara, H. Fujimoto, H. Itoi, K. Nomura, H. Tanaka, M. T. Miyahara, P. A. Bonnaud, R. Miura, A. Suzuki, N. Miyamoto, N. Hatakeyama, A. Miyamoto, K. Ikeda, T. Otomo, T. Kyotani, *Carbon* **2018**, *129*, 854–862.
[22] E. E. Taylor, K. Garman, N. P. Stadie, *Chem. Mater.* **2020**, *32*, 2742–2752.
[23] N. P. Stadie, S. Wang, K. V. Kravchyk, M. V. Kovalenko, *ACS Nano* **2017**, *11*, 1911–1919.
[24] R. J. Dubey, J. Nussli, L. Piveteau, K. V. Kravchyk, M. D. Rossell, M. Campanini, R. Erni, M. V. Kovalenko, N. P. Stadie, *ACS Appl. Mater. Interfaces* **2019**, *11*, 17686–17696.
[25] R. J. Dubey, T. Colijn, M. Aebli, E. E. Hanson, R. Widmer, K. V. Kravchyk, M. V. Kovalenko, N. P. Stadie, *ACS Appl. Mater. Interfaces* **2019**, *11*, 39902–39909.
[26] K. Matsuoka, Y. Yamagishi, T. Yamazaki, N. Setoyama, A. Tomita, T. Kyotani, *Carbon* **2005**, *43*, 876–879.
[27] Z. Ma, T. Kyotani, A. Tomita, *Carbon* **2002**, *40*, 2367–2374.
[28] S. J. Gregg, K. S. W. A. Sing, *Adsorption, Surface Area and Porosity*, **1982**, 2nd ed., Academic Press, New York.
[29] S. Wang, K. V. Kravchyk, A. N. Filippin, U. Muller, A. N. Tiwari, S. Buecheler, M. I. Bodnarchuk, M. V. Kovalenko, *Adv. Sci.* **2018**, *5*, 1700712.
[30] S. Wang, K. V. Kravchyk, A. N. Filippin, R. Widmer, A. N. Tiwari, S. Buecheler, M. I. Bodnarchuk, M. V. Kovalenko, *ACS Appl. Energ. Mater.* **2019**, *2*, 974–978.
[31] R. Rowsey, E. E. Taylor, S. Irle, N. P. Stadie, R. K. Szilagyi, *J. Phys. Chem. A* **2021**, *125*, 6042–6058.
[32] N. Mardirossian, M. Head-Gordon, *J. Chem. Theory Comput.* **2016**, *12*, 4303–4325.
[33] E. Jonsson, P. Johansson, *Phys. Chem. Chem. Phys.* **2015**, *17*, 3697–3703.
[34] J. B. Goodenough, K. S. Park, *J. Am. Chem. Soc.* **2013**, *135*, 1167–1176.
[35] S. J. An, J. Li, C. Daniel, D. Mohanty, S. Nagpure, D. L. Wood, *Carbon* **2016**, *105*, 52–76.
[36] M. Ue, M. Takeda, M. Takehara, S. Mori, *J. Electrochem. Soc.* **1997**, *133*, 2684–2688.
[37] K. Xu, *Chem. Rev.* **2004**, *104*, 4303–4418.
[38] O. Borodin, W. Behl, T. R. Jow, *J. Phys. Chem. C* **2013**, *117*, 8661–8682.
[39] J. B. Haskins, W. R. Bennett, J. J. Wu, D. M. Hernandez, O. Borodin, J. D. Monk, C. W. Bauschlicher, Jr., J. W. Lawson, *J. Phys. Chem. B* **2014**, *118*, 11295–11309.
[40] M. T. Ong, O. Verners, E. W. Draeger, A. C. van Duin, V. Lordi, J. E. Pask, *J. Phys. Chem. B* **2015**, *119*, 1535–1545.
[41] E. O. Stejskal, J. E. Tanner, *J. Chem. Phys.* **1965**, *42*, 288–292.

Manuscript received: October 1, 2022
Revised manuscript received: November 6, 2022
Accepted manuscript online: November 9, 2022
Version of record online: November 28, 2022

RESEARCH ARTICLE

Storage space: Guidelines for fast and high-density anion storage in microporous carbon materials are deduced by systematic variation of the anion size, shape, and type, as well as by variation of the solvent and overall electrolyte composition (i.e., salt concentration). An upper limit of two anions stored per 1.2 nm micropore "supercage" is presented.

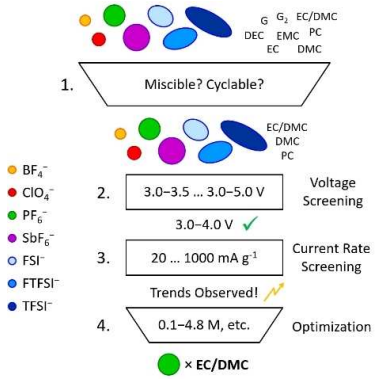

C. Welty, E. E. Taylor, S. Posey, P. Vailati, Dr. K. V. Kravchyk, Prof. M. V. Kovalenko, Prof. N. P. Stadie**

1 – 12

Methodological Studies of the Mechanism of Anion Insertion in Nanometer-Sized Carbon Micropores